OPEN ACCESS
IOP Publishing

Plasma Physics and Controlled Fusion

Plasma Phys. Control. Fusion **67** (2025) 075011 (10pp)

https://doi.org/10.1088/1361-6587/ade008

Development of high-current baseline scenario for high deuterium–tritium fusion performance at JET

L Garzotti[1,*], D Frigione[2], P Lomas[1], F Rimini[1], D Van Eester[3], S Aleiferis[1], E Alessi[4], F Auriemma[5], I S Carvalho[6], P Carvalho[1], A Chomiczewska[7], E De La Luna[8], D R Ferreira[6], A Field[1], M Fontana[1], L Frassinetti[9], S Gabriellini[10], Z Ghani[1], E Giovannozzi[11], C Giroud[1], W Gromelski[7], I Ivanova-Stanik[7], V Kiptily[1], K Kirov[1], M Lennholm[1], C Lowry[1], C F Maggi[1], J Mailloux[1], S Menmuir[1], R B Morales[1], S Nowak[4], V Parail[1], A Patel[1], A Pau[12], C Perez von Thun[7], L Piron[13], G Pucella[11], C Reux[14], O Sauter[12], E R Solano[8], C Sozzi[4], Ž Štancar[1], C Stuart[1], H Sun[1], G Telesca[7], D Tskhakaya[15], M Valovič[1], N Wendler[7], V K Zotta[10] and JET Contributors[16]

[1] United Kingdom Atomic Energy Authority, Culham Campus, Abingdon, Oxon OX14 3DB, United Kingdom
[2] Università di Roma Tor Vergata,Via del Politecnico 1, Roma, Italy
[3] Laboratory for Plasma Physics LPP-ERM/KMS, B-1000 Brussels, Belgium
[4] Institute for Plasma Science and Technology, CNR, via R. Cozzi 53, 20125 Milano, Italy
[5] Consorzio RFX, Corso Stati Uniti 4, 35127 Padova, Italy
[6] Instituto de Plasmas e Fusão Nuclear, Instituto Superior Técnico, Universidade de Lisboa,1049-001 Lisboa, Portugal
[7] Institute of Plasma Physics and Laser Microfusion, Hery 23, 01-497 Warsaw, Poland
[8] Laboratorio Nacional de Fusión, CIEMAT, Madrid, Spain
[9] Fusion Plasma Physics, EECS, KTH Royal Institute of Technology, SE-10044 Stockholm, Sweden
[10] Dipartimento di Ingegneria Astronautica, Elettrica ed Energetica, SAPIENZA Università di Roma,Via Eudossiana 18, 00184 Roma, Italy
[11] Dip.to Fusione e Tecnologie per la Sicurezza Nucleare, ENEA C. R. Frascati, via E. Fermi 45, 00044 Frascati (Roma), Italy
[12] Ecole Polytechnique Fédérale de Lausanne (EPFL), Swiss Plasma Center (SPC), CH-1015 Lausanne, Switzerland
[13] Dipartimento di Fisica 'G. Galilei', Università degli Studi di Padova, Padova, Italy
[14] CEA, IRFM, F-13108 Saint Paul Lez Durance, France
[15] Institute of Plasma Physics of the CAS, Za Slovankou 1782/3, 182 00 Praha 8, Czech Republic

E-mail: luca.garzotti@ukaea.uk

Received 14 March 2025, revised 28 April 2025
Accepted for publication 3 June 2025
Published 26 June 2025

CrossMark

[16] See the author list of Overview of T and D-T results in JET with ITER-like wall by C F Maggi *et al* published in Nuclear Fusion Special Issue: Overview and Summary Papers from the 29th Fusion Energy Conference (London, UK, 16–21 October 2023).

* Author to whom any correspondence should be addressed.

Abstract

The development of a high current baseline scenario ($I_p = 3.5MA$, $q_{95} \approx 3.0$, $\beta_N < 2$) in deuterium (D), tritium (T) and deuterium–tritium (D–T) for high D–T fusion performance at JET with Be/W wall is described. We show that a suitable scenario capable of delivering up to 10 MW of fusion power, depending on the auxiliary heating power available, was successfully developed in D. However, when translated to T and D–T, the same scenario could not be sustained for the target duration of 5 s due to the impossibility to achieve the stationary compound edge localized modes regime necessary to flush the tungsten (W) from the plasma and control the density. Nevertheless, a peak fusion power in the order of 8 MW, with 60% of the power coming from thermal fusion reactions, was obtained in D–T at 3.5 MA, with ≈30 MW of neutral beam injection heating and 3–4 MW of ion cyclotron resonance heating, in line with the predictions obtained with the JINTRAC integrated scenario modelling suite of codes equipped with the QuaLiKiZ transport model and based on the extrapolation of the performance of similar D plasmas.

Keywords: JET, tokamak, magnetic confinement, nuclear fusion power, deuterium–tritium

1. Introduction

Deuterium–tritium (D–T) plasma experiments producing significant fusion power were first performed on JET in 1997 during an experimental campaign denominated DTE1, when 16.1 MW of peak fusion power were achieved transiently in an edge localized modes (ELM)-free, hot-ion H-mode plasma and over 4 MW of fusion sustained for 5 s in a stationary type-I ELM H-mode plasma [1, 2]. Experiments in DTE1 were carried out with a carbon (C) wall and indicated that the T retention was unacceptable for a tokamak such as ITER.

For this reason, it was decided to equip JET with a beryllium (Be) wall and a tungsten (W) divertor and perform a second D–T campaign, DTE2, with the new machine configuration. Meanwhile, several other upgrades were implemented. Most importantly, the neutral beam injection (NBI) power was increased from 24 MW available in DTE1 to (nominally) 34 MW in DTE2 and a number of new diagnostics were installed, such as a high resolution Thomson scattering [3] to measure the electron density and temperature profiles with higher spatial and temporal resolution compared to the LIDAR used in 1997 and a series of neutron diagnostic, including an array of high-resolution D–T neutron spectrometers to diagnose in detail the spectrum of the D–T neutrons and a unique alpha-particle diagnostics to measure confined and lost D–T alphas [4, 5].

One of the scientific objectives of DTE2 was to demonstrate fusion power in excess of 10 MW sustained for 5 s. To this aim two main scenarios were developed testing two different approaches to high fusion power and relying on different physics: the baseline scenario ($I_p = 3.5$ MA, $q_{95} \approx 3.0$, $\beta_N < 2$), relying on high plasma current and stronger poloidal magnetic field to achieve good confinement and the hybrid scenario ($I_p \leqslant 3.0$ MA, $q_{95} \approx 4.8$, $\beta_N > 2$) [6], featuring lower plasma current and taking advantage at the same time of the higher β_N and optimized q profile for improved MHD stability to obtain good confinement. In addition, a tritium-rich version of the hybrid scenario was developed [7], where the plasma composition, NBI and ion cyclotron resonance heating (ICRH) were optimized in order to inject D neutral beams in a T-rich plasma to maximize the beam-target reaction rate and, at the same time, exploit the fundamental D heating of the minority D beam ions to maximize the NBI/ICRH synergy and further boost the fusion power.

Despite each scenario having its specific characteristics and challenges, all scenarios operate in H-mode exhibiting either type-I (hybrid scenario) or compound (baseline scenario) ELMs expelling particles and heat from the plasma in bursts. Similarly, all scenarios rely on high auxiliary heating power, typically ≈ 32 MW of NBI and ≈ 4 MW of ICRH. In addition, all scenarios are affected by high-Z impurity accumulation, the most dangerous of which is W originating in the divertor region of the Be/W wall.

In this paper we concentrate on the analysis of the baseline scenario, describe its development in D, T and D–T and present the results in terms of fusion power achieved and the stationarity of discharge. The scope of the paper is to provide an overview of the experimental achievements, the challenges faced and the lesson learned in pursuing them. Specific issues that require a more in-depth analysis and explanation are or will be addressed in specific papers, some of which are referenced here. To illustrate the characteristic of the scenario in D, T and D–T we have selected one representative shot at 3.5 MA/3.35 T per isotope. This is justified by the fact that, despite the staged approach in terms of current increase in D, in T and D–T the baseline scenario was operated only at these values of plasma and field. Therefore, a comparison between all isotope masses is only possible at 3.5 MA/3.35 T. Moreover, we were interested in comparing only the few highest performance plasmas in D with their counterparts in T and D–T. High performance plasmas at high current were not frequent, because of the optimization process required to achieve them and the fact that they required all the heating and fuelling systems (NBI, ICRH and pellet injector) working at maximum performance for the whole duration of the discharge without any off-normal event (such as, for example, hot spots on the plasma facing components or sudden impurity injection events) causing the request of termination of the shot from the tokamak protection system or, even worse, a disruption. In the end fewer than five D plasmas, all similar between them, with the potential to deliver $\sim$10 MW of fusion power were obtained, which justify our approach to select only one representative shot per isotope.

2. Development of the baseline scenario in D

The development of the baseline scenario in D with the new JET configuration started immediately after the installation of the JET Be/W wall and was carried out over several years. One of the main challenges was to recover the good confinement properties characteristic of equivalent baseline plasmas with the JET C wall [8, 9]. This was achieved mainly by optimizing the fuelling scheme using ELM pacing pellets and low gas puffing to minimize the particle throughput. It is important to note that one of the main consequences of transitioning from a full C wall to a Be/W wall is that the fuelling scheme developed in a C machine cannot be directly translated to the same machine when equipped with a metal wall. In the first case the wall acts as particle reservoir and, depending on the wall condition and the quantity of main gas trapped in the plasma facing components, can contribute significantly to the plasma fuelling and isotope composition, whereas, because of the lower fuel retention, with a Be/W wall the fuelling is controlled more directly and reproducibly by the gas inlet system.

The optimization process started at moderate plasma current and toroidal field (2.5 MA/2.4 T) to establish a low edge collisionality, high pedestal pressure, good confinement plasma in D, maximizing the neutron rate. From there we increased the current I_p and toroidal field B_T in steps to 3.0 MA/2.8 T, 3.5 MA/3.35 T, 3.8 MA/3.6 T and, finally, to 4 MA/3.6 T (consequently, changing q_{95} from $\approx$3 to $\approx$2.7). This stepwise increase in I_p and B_T is similar to the strategy initially outlined in the ITER Research Plan within the Staged Approach and now abandoned [10, 11].

The idea of minimizing the particle throughput stems from the fact that it is observed experimentally and, for type-I ELM plasmas, interpreted in the light of MHD stability and kinetic profile analysis [12], that the best plasma performance in terms of energy confinement, pedestal pressure and neutron rate is obtained at the lowest achievable values of plasma density at the separatrix. For the baseline scenario this was achieved by positioning the outer divertor leg as close as possible to the entrance of the pumping duct and using a combination of ELM pacing pellets and the lowest gas dosing compatible with maintaining the ELM activity necessary to flush the W and control the density. In fact, in JET Be/W wall it was found that a low triangularity corner divertor configuration, with the strike points at the optimum pumping positions [13], displays superior confinement to the high triangularity configuration that had shown best high density confinement in JET with a C wall [14]. In all baseline plasmas, to avoid overheating the divertor targets, the strike point was swept with an amplitude of ~ 3 cm and a frequency of 4 Hz. This could influence the L–H power threshold as shown by previous experiments with stationary strike-point locations indicating that, for typical type-I ELM conditions the L–H power transition threshold increases with increasing strike-point major radius [15].

For a typical baseline plasma at 3.5 MA/3.35 T, the minimum particle throughput was achieved by the injection of small ELM-pacing pellets at 45 Hz during the L–H transition, reduced to 35 Hz during the H-mode phase and resulting in a nominal particle throughput of 1.70×10^{22} el s^{-1} and 1.32×10^{22} el s^{-1} respectively, combined with gas-puff rate during the main heating phase of $\sim 1.0 - 1.5 \times 10^{22}$ el s^{-1}. The choice to inject pellets was motivated by the observation that pellet injection allowed the achievement of a stationary discharge at a lower total particle throughput with respect to gas puff alone, therefore reducing the detrimental effect of higher fuelling on confinement. The pellet injection frequency was motivated by the limits of the JET high-frequency pellet injector performance (50 Hz) and the residual gas was necessary because operation in D showed that pellet-only fuelled plasmas did not result in a stationary discharge. The choice of a 50–50 pellet-gas particle throughput was made in view of substituting D gas puff with T in D–T plasmas to achieve a 50–50 D–T fuelling rate, which could be subsequently fine tuned, depending on the different fuelling efficiencies of gas and pellet, to obtain a 50–50 D–T plasma composition as predicted by modelling performed in preparation for the D–T experiments [16].

In addition to the optimized fuelling scheme, another essential ingredient required to achieve a high neutron rate in the baseline scenario was an adequate amount of additional heating power. At 3.5 MA/3.35 T, at which most of the scenario development in D was carried out, NBI power $\geqslant$28 MW and ICRH power $\geqslant$3 MW (51 MHz, H minority heating scheme) was necessary to maintain the plasma in H-mode and prevent the accumulation of W in the plasma core. Unfortunately, due to the limited reliability of the NBI system at the time, these conditions were reached only in 16 of the 57 shots at 3.5 MA in our database.

In DTE2, for the baseline scenario, after the upgrade of the NBI heating system, all sixteen NBI injectors were operated at an energy of 110 keV and with a beam energy composition of $\sim$53% full energy, $\sim$34% half energy and $\sim$13% one third energy in D and $\sim$57% full energy, $\sim$27% half energy and $\sim$14% one third energy in T. In DTE1 eight NBI injectors were operated at 80 keV (always in D) with a beam energy composition of $\sim$83% full energy, $\sim$13% half energy and $\sim$4% one third energy and eight were operated at 140 keV with a beam energy composition of $\sim$60% full energy, $\sim$20% half energy and $\sim$20% one third energy in D and $\sim$71% full energy, $\sim$16% half energy and $\sim$13% one third energy in T. The details of the physics of the NBI heating are beyond the scope of this paper, but, in general, in DTE2 the NBI power deposition was more peripheral than in DTE1 both for electrons and ions and both in D and D–T.

As for the ICRH heating, in DTE2 the H minority scheme was adopted instead of the ^{3}He minority scheme used in DTE1, despite the latter is expected to result in a higher fraction of the heating power going to the ions and therefore in better fusion performance. The main reason behind this choice is the limited duration of DTE2 and number of experimental sessions dedicated to the development of the baseline scenario and the amount of time that would have been required to clean the machine from the residual ^{3}He in preparation for other experiments in the programme that could not be performed with residual ^{3}He. Indeed seven shots with ^{3}He minority heating were performed at 3.5 MA/3.28 T in D, albeit with the NBI power $\leqslant 25$ MW and without optimized fuelling, but no significant differences in the ion temperature were observed [17]. Therefore, no further optimization of the ^{3}He minority scheme was attempted and the scheme was not used when the scenario was developed in T and D–T where the time constrains were even stricter than in D.

The main parameters of JET pulse number (JPN) 96893, one of the best stationary shots in D at 3.5 MA in terms of average neutron yield over 5 s, are shown in figure 1, where we plot the NBI and ICRH heating power, the bulk plasma radiated power, the core and edge line averaged plasma electron density, the core ion and electron temperature, the BeII emission (indicative of the plasma ELM activity), the plasma diamagnetic energy content, the normalized β, the gas fuelling rate and the total neutron yield. In this discharge, at 3.5 MA/3.35 T with injected power of $\sim$28 MW of NBI and $\sim$3.7 MW of ICRH, $H_{98} \sim 0.89$ and an average neutron yield of $\sim 2.6 \times 10^{16}$ neutrons/s were obtained for 5 s. A simple extrapolation of this pulse to an equivalent 50–50 D–T plasma, assuming the same kinetic profiles and neglecting possible isotope effects, gives $\sim$8.8 MW of peak fusion power and 7.0 MW averaged over 5 s.

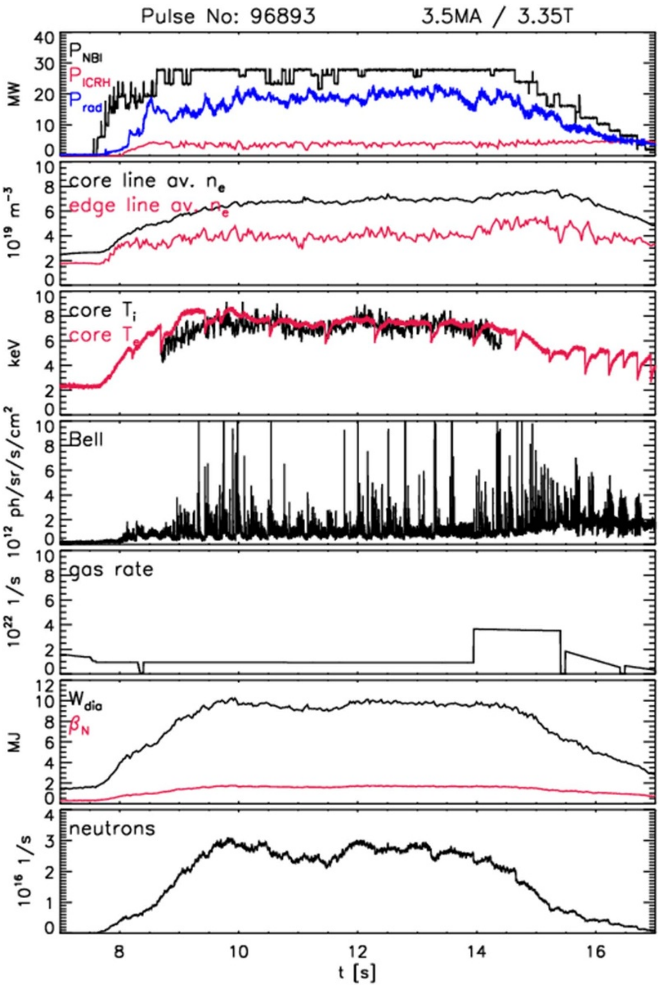

Figure 1. Time traces for the JPN 96893, a high-performing, stationary JET baseline plasma in D at 3.5 MA/3.35 T. ELM pacing pellets (mass 3.77×10^{20} D atoms and frequency 45 Hz, reduced to 35 Hz at 8.5 s are injected between 7.5 s and 14 s.

The compound ELM regime resulting from the fuelling scheme described earlier is illustrated in figure 2, where we show the D_α light coming from the pellet ablation and the BeII emission indicating the ELM activity from JPN 96893. It can be seen that the ELMs are not regular type-I ELM with a well-defined frequency, but rather of a compound type with large ELMs followed by trains of smaller ones. The pellet ELM triggering efficiency is 50% and it is typical for this plasma current. Note that the presence of compound ELMs makes the interpretation, analysis and modelling of the physics underlying the behaviour of the pedestal particularly challenging, since present understanding of the pedestal applies mainly to type-I ELM plasmas.

Despite the fact that a direct parallel between the two pulses is not straightforward, when compared with JPN 42464 [18], JPN 96893 shows a higher plasma stored energy (10 MJ versus 8 MJ) and a higher radiated power ($\geqslant 10$ MW versus ~ 4.5 MW). It should also be noted that JPN 42464 had $I_\mathrm{p} = 3.8$ MA and $B_\mathrm{T} = 3.8$ T and was heated with ~ 18 MW of NBI and 0.5 MW of ICRH in ^{3}He minority heating scheme, as opposed to the H minority heating scheme used in JPN 96893. TRANSP [19] analysis indicates that the energy confinement time in JPN 96893 was $\tau_\mathrm{E} \sim 0.3$ s [20] compared with $\tau_\mathrm{E} \sim 0.4$ s in JPN 42464 (corresponding to $H_{98} \sim 0.9$) [21]. As mentioned above, another difference between JPN 42464 and JPN 96893 is the nature of the ELMs. JPN 42464 exhibits regular type-I ELMs, whereas JPN 96893, as all baseline shots at 3.5 MA with Be/W wall, is characterized by compound ELMs of the type shown in figure 2. JPN 42464 is the D counterpart of JPN 42982, the D–T pulse with the best sustained performance in DTE1.

The reason for the difference in ELM type is not clear and is being investigated. In particular, dedicated analysis aiming at disentangling the effects of the margin above the L–H transition power threshold and the effects of the fuelling scheme and the wall material on the pedestal kinetic profiles and MHD stability is under way and the results will be published in a dedicated paper.

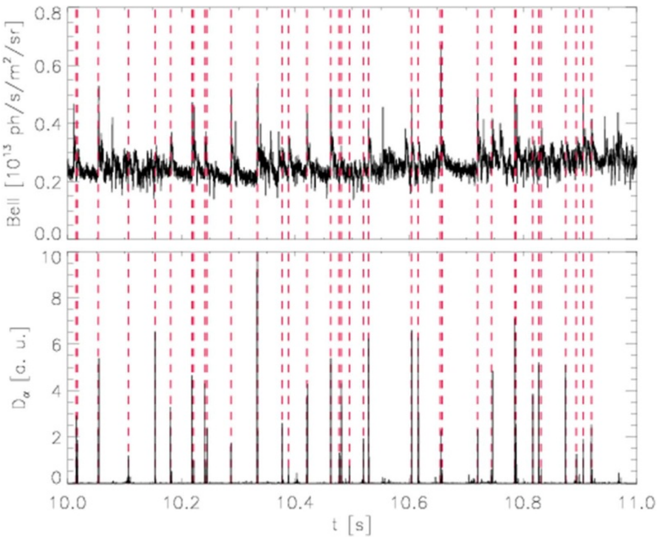

Figure 2. Compound ELM regime in a baseline plasma in D at 3.5 MA/3.35 T (JPN 96893). Top: BeII emission indicating the ELM activity. Bottom: D_α emission marking the pellet ablation. The vertical red dashed lines help identify whether a pellet triggers an ELM or not.

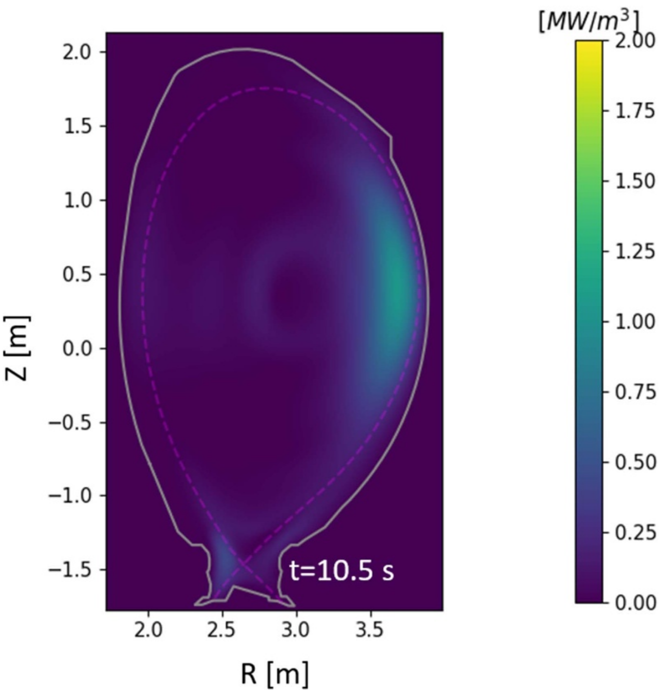

Figure 3. Radiated power density from bolometric inversion for JPN 96893 at $t = 10.5$ s. The radiation is emitted from the LFS of the plasma throughout the entire flat-top and W does not accumulate on the magnetic axis.

It should be noted that in JET baseline plasmas with a Be/W wall the impurity-induced radiation remains localized on the low field side. This is evident from bolometric tomographic inversion as shown in figure 3 for a typical baseline plasma. The radiation from this region is normally steady, as long as the ELM activity lasts, and the impurities do not accumulate in the centre due to the combination of the flat density profiles suppressing neo-classical inward convection and ion temperature gradient screening boosted by the ICRH power as described in [22]. Moreover, recent modelling work has identified an operational window of enhanced neoclassical screening driven by strong rotation at low collisionality [23, 24], which can also contribute to explaining the lack of core W accumulation found in the baseline scenario at low gas with pellets.

Attempts to increase the plasma current from 3.5 MA to 3.8 MA and 4 MA were hindered by the fact that reliable NBI power in excess of 30 MW (necessary to operate at higher plasma current) was not routinely available and losses of heating power during the flat-top resulted in disruptions that were deemed too dangerous for the integrity of the machine. For these reasons, as a compromise between exploring the desired high current regime and the objective operational limits of the machine, the decision was taken to develop the baseline scenario in T and D–T at 3.5 MA/3.35 T.

3. Development of the baseline scenario in T

The development of the baseline scenario in T was motivated by the necessity to investigate the effects of the isotope mixture on the physics underpinning the scenario, explore isotope effects that can compromise the performance in D–T and anticipate the changes that might be needed to recover the performance obtained in D. It should be noted that, since the JET pellet injector cannot operate in T and D pellets could not be used in T plasmas to avoid unwanted D–T reactions unnecessarily consuming the finite JET D–T neutron budget, the impact of the higher isotope mass on the baseline scenario could only be tested either with gas puff only or by using H pellets.

Initially, the scenario was run in T at 3 MA without pellets and with T gas puff only at 2.7×10^{22} el s^{-1}. However, this fuelling scheme resulted in an ELM free plasma that exhibited line average density and radiated power increasing after the L–H transition and could not be sustained for more than 1 s in H-mode. Therefore, it was decided to increase the plasma current to 3.5 MA, to operate at the same current as in D and use H ELM pacing pellet of the same size as the pellets used in D to promote the ELM activity needed for W flushing and keep the discharge stationary. In T, to avoid excessive H contamination of the plasma, the pellet frequency was limited between 15 Hz and 25 Hz resulting in a H concentration reaching a stationary value between 10% and 15% in $\sim$1 s. It should be noted that it was more challenging than anticipated to deliver steady high NBI power in T and only three pulses with NBI power $\geqslant$28 MW were obtained at 3.5 MA/3.35 T.

Despite the lower frequency the H pellets triggered ELMs with an 50%–60% efficiency and improved the stationarity of the pulse. However, even with the injection of H pellets, we did not succeed in sustaining the plasma in H-mode for more than 2.5 s. Also at 3.5 MA/3.35 T all T plasmas could not be sustained for the entire programmed duration of the flat-top ($\sim$5 s) and the T plasma sustained for the longest time is presented in figure 4, where we show the same traces as in figure 1 for

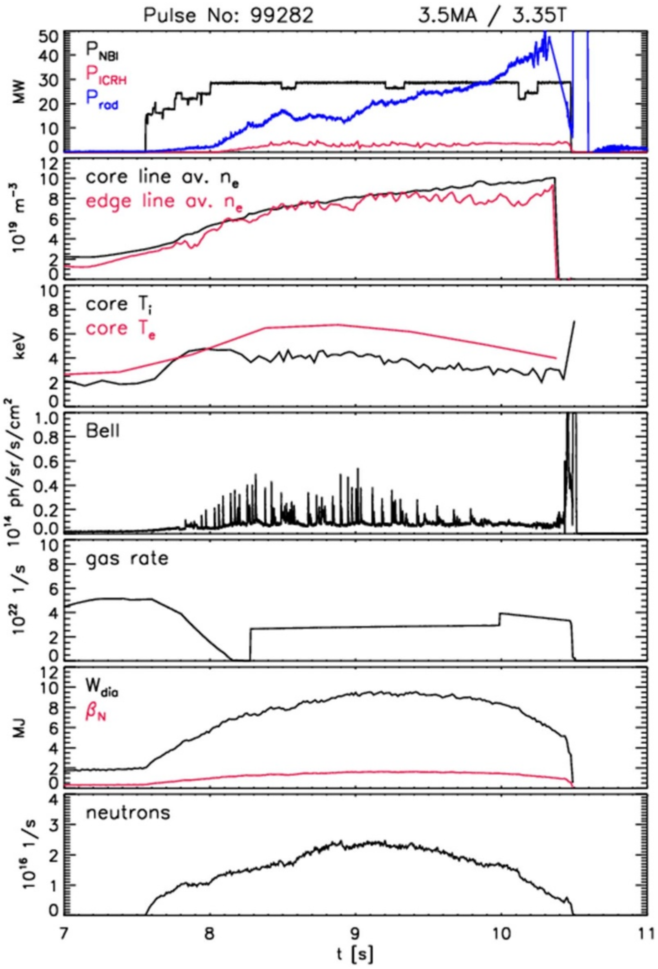

Figure 4. Time traces for the JPN 99282, the JET baseline plasma in T with H pellet injection sustained for the longest time at 3.5 MA/3.35 T. ELM pacing pellets (mass 3.77×10^{20} H atoms and frequency 25 Hz, reduced to 17 Hz at 8.8 s are injected from 7.5 s until the disruption occurs.

JPN 99282 (with the exception that, due to the unavailability of the high-resolution Thomson scattering, the core electron temperature in the plot is from the LIDAR Thomson scattering). In this T pulse 28 MW of NBI power and 3.5 MW of ICRH power were injected in the plasma and H pellets were injected at 25 Hz until $t = 8.8$ s and at 17 Hz thereafter.

It is clear that even in this case the plasma density steadily increases, the ELM activity disappears, the radiated power overtakes the total heating power, the plasma falls back into L-mode and the discharge eventually disrupts. We interpret this result as a consequence of the better particle confinement in T with respect to D [25], leading to a chain of events involving increasing density, weakening ELM activity controlling the density and flushing the W at the applied fuelling rate, increasing radiated power and eventually a radiative collapse of the plasma associated with a H–L transition.

Notwithstanding the fact that we could not establish a stationary baseline plasma at 3.5 MA/3.35 T within the amount of time allocated to T operation, the decision was made to operate the baseline scenario in D–T at the same plasma current and magnetic field. This was justified by the fact that we wanted to explore the confinement in D–T at the highest current realistically achievable in D for the baseline scenario and that the hybrid scenario already operated at lower current (2.3 MA). Moreover, we expected that the possibility of injecting D ELM pacing pellets at higher frequency, the availability of higher and more reliable NBI power coming from the D beams and a lower particle confinement in D–T than in T would allow us to maintain the compound ELM regime, prevent the density increase and achieve a stationary discharge for the target duration of 5 s.

4. Development of the baseline scenario in D–T

The scenario development in D–T consisted of 14 baseline shots at 3.5 MA/3.35 T, of which 7 were technically successful (i.e. all heating and fuelling systems performed as requested), with injected NBI power between 26 and 29 MW and ICRH power 3-4 MW. It should be noted that none of the baseline shot in D–T could be sustained for more than 3 s. In order to save neutron and T budget and to prevent disruptions, some shots were stopped early either by a 'dud' detection system (when H_{98} or the ratio between the neutron rate and the plasma stored energy squared were below a certain threshold) [26] or by the plasma protection system (when $P_{\mathrm{NBI}} < 26$ MW or $f_{\mathrm{rad}} > 0.7$, where f_{rad} is the radiated power fraction defined as bulk radiated power divided by total auxiliary heating power). However, even when NBI heating power $\geqslant$28 MW was available, similarly to the T plasmas, the intensity of the compound ELM activity was decreasing and the line average density and the density at the top of the pedestal were increasing steadily during the flat-top phase leading to increased radiation, complete cessation of the ELM activity at the applied fuelling rate and eventually to a radiative collapse of the discharge associated with a H–L transition. In order to promote the ELM activity and achieve sustained fusion power for 5 s we tried increasing the D and T gas puff rate by 0.3×10^{22} el s^{-1} and 0.4×10^{22} respectively after $t =$ 9 s, but this was not enough to recover the behaviour observed in D. It is conceivable that an even higher increase in fuelling rate, which we could not try for lack of experimental time, might have been sufficient to stabilize the scenario for 5 s albeit at the price of a significant deterioration of the fusion performance.

The main parameters of JPN 99948, the best baseline shot in D–T in terms of duration and peak fusion power, are shown in figure 5, where we plot the same time traces as in figure 1 and included the generated fusion power alongside the NBI and ICRH additional heating power and the radiated power. In this discharge, at 3.5 MA/3.35 T with injected power of $\sim$29 MW of NBI and $\sim$3.7 MW of ICRH, $H_{98} \sim 0.91$ and fusion power of 7.84 MW were obtained on average for $\sim$2 s before the radiative collapse of the plasma. A peak fusion power of 8.3 MW was obtained in line with the extrapolations from D plasmas.

A 50–50 D–T mixture was obtained as a result of 50–50 D–T NBI, injection of D pellets of mass 3.77×10^{20} atoms at a

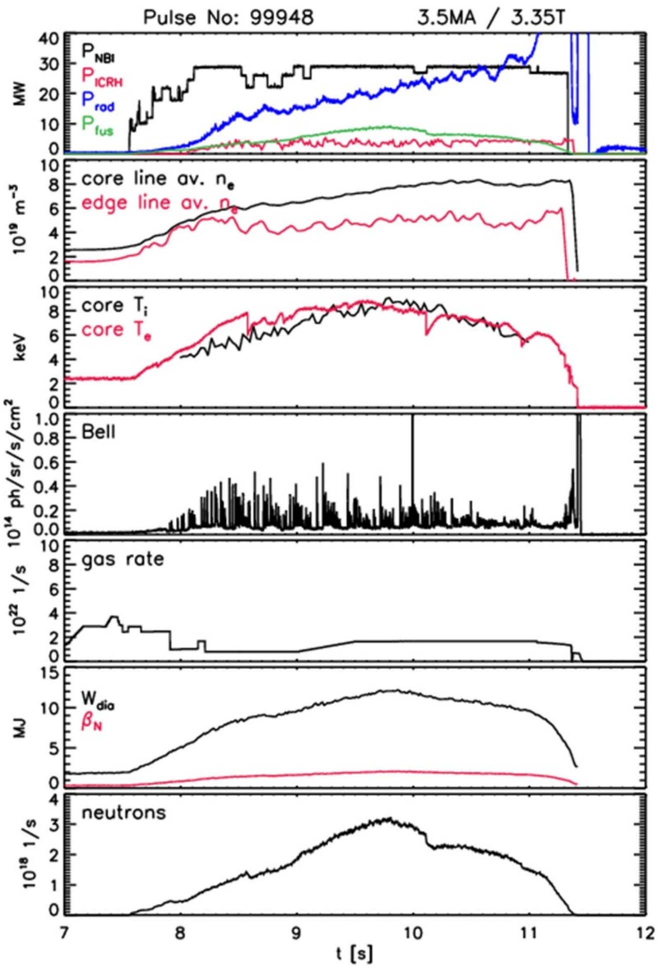

Figure 5. Time traces for the JPN 99948, the JET baseline plasma in D–T with the highest peak fusion performance and sustained for the longest time at 3.5 MA/3.35 T. ELM pacing pellets (mass 3.77×10^{20} D atoms and frequency 45 Hz) are injected from 7.5 s until the disruption occurs.

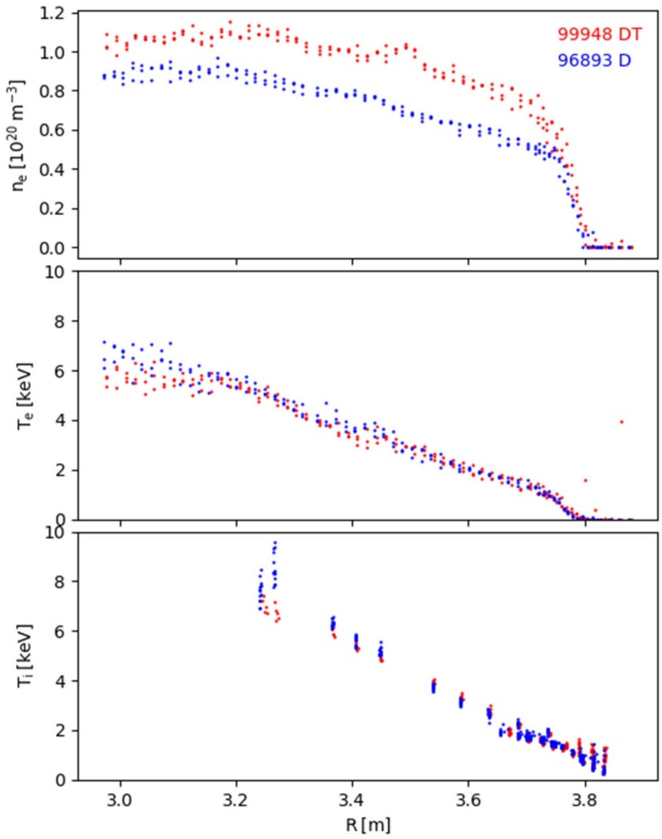

Figure 6. Comparison of electron density (top), electron temperature (middle) and ion temperature (bottom) profiles at $t = 10$ s for JPN 99948 (DTE2, D–T) and JPN 96893 (D). Both pulses are at 3.5 MA/3.35 T.

frequency of 45 Hz. T was puffed at a rate of 0.8×10^{22} el s^{-1} until $t = 9$ s and increased to 1.5×10^{22} el s^{-1} over 0.5 s thereafter. The increase in T throughput was matched with a similar increase in D gas puff. The motivation for increasing the particle throughput after 9 s was to try and maintain the ELM activity for longer (ideally 5 s) after having accessed the H-mode at low separatrix density and good plasma performance.

TRANSP analysis indicates that in JPN 99948 60% of the fusion power was generated by thermal fusion reaction and 40% from beam-plasma reactions and the total alpha heating was around 1.5 MW. The same TRANSP analysis shows that the fast particle density fraction in these high-current high-power D–T baseline plasmas was ∼20%.

Further insight in the dynamics of baseline plasmas in D–T can be obtained if we compare the density and temperature profiles of JPN 99948 (D–T) with the profiles of JPN 96893 (D). This is done in figure 6, where we show that, despite entering the H mode with similar density and temperature profiles, at $t = 10.5$ s, just before the start of the radiative collapse, the electron density is significantly higher in D–T than in D, whereas the electron and ion temperature are similar for the two isotopes.

Comparing this pulse with JPN 42982 that produced 4 MW of fusion power in DTE1, we notice a higher plasma stored energy (12 MJ at peak performance in 99948 versus an average of 10.5 MJ in 42982). The radiated power increases steadily from 10 MW to ∼15 MW during the first 2.5 s of the H-mode phase and finally diverges more rapidly to >30 MW in the last 0.35 s before the disruption, caused by radiative collapse. This compares to an inter-ELM radiated power of ∼5.6 MW in JPN 42982. It should also be noted that JPN 42982 had ∼22 MW of NBI and 2 MW of ICRH in ^{3}He minority heating scheme as opposed to H minority heating scheme in JPN 99948. TRANSP analysis [20] indicates that the confinement time in JPN 99948 was $\tau_E \sim 0.35$ s compared with $\tau_E \sim 0.4$ s in JPN 42982 (corresponding to $H_{98} \sim 0.89$) [21].

5. Discussion

The development of a baseline scenario at the highest plasma current achievable on JET in DTE2, given the available heating power, demonstrated that, although a scenario capable of delivering $P_{fus} \leqslant 10$ MW for 5 s when extrapolated to D–T with enough additional heating power was achieved in D, the same scenario could not be sustained for more than 1–2 s in

T and 3 s in D–T. The physics interpretation of this results is based on the different behaviour of the ELM activity and the plasma density depending on the plasma isotopic composition. In D, inter-ELM particle transport and ELM activity combine to deliver a stationary plasma density that does not increase with time. As a consequence, the radiated power remains constant. With a total heating power ∼32 MW, at 3.5 MA and 3.35 T the plasma remains in H-mode and the whole discharge is stationary over a 5 s time window. In T and D–T, where the particle transport is reduced, the plasma density builds up between ELMs and the ELM activity, at the same fuelling rate, is not sufficient to flush the main hydrogenic gas and the W, resulting in a radiated power from the low field side of the plasma increasing over time and eventually in the radiative collapse of the discharge. It is worth noting that, despite the expected higher W sputtering induced by T with respect to D, the W concentration in the plasma, estimated from the quasi-continuum emission of W^{27+}–W^{35+} ions, was similar between D and D–T and $\leqslant 10^{-4}$.

This interpretation explains also why in DTE1 a high-current baseline scenario could be sustained for 5 s. Indeed, the lack of W and the presence of type-I ELMs preventing the secular increase in the density meant that the radiated power was constant and in the region of 4–5 MW, as opposed to >10 MW and increasing with time in DTE2, ensuring that the plasma would not undergo a radiative collapse.

This point is further illustrated in figure 7, where we compare the electron density and the electron and ion temperature profiles 3 s after the start of the main heating phase for JPN 99948 (DTE2 in D–T) and JPN 42982 (DTE1 in D–T). It can be seen that, with respect to JPN 42982, JPN 99948 has higher on-axis and pedestal density and lower electron and ion temperatures outside $\sqrt{\psi_N} > 0.5$. A similar comparison between profiles of JPN 42464 (in D) and 42982 (DTE1 in D–T) shows a much closer similarity and both sets of profiles (42464 and 42 982) are similar to JPN 96893 (in D).

Despite the fact that it could not be sustained for the reasons explained above, the peak fusion performance achieved in the baseline scenario is in line with, and even exceeding, the predictions of state-of-the-art transport models performed before the start of DTE2. This is shown in figure 8 where we compare the peak P_{fus} obtained in the baseline scenario at 3.5 MA (including two extra shots at 3 MA) with the predictions obtained before DTE2 with the JINTRAC integrated modelling suite [27]. The simulations were based on baseline H-mode plasmas in D at $\beta_N \sim 1.8$ [28] and used the QuaLiKiZ transport model [29] to estimate the fusion power achievable for different plasma currents and levels of additional heating power. It is clear from the picture how the baseline scenario was severely hindered by the lack of reliable total heating power above 33 MW, which, beside limiting the achievable fusion power, prevented operations at higher plasma current. Nevertheless, the good agreement between predicted and actual peak performance gives us confidence in the extrapolation capabilities of available transport models towards future experiments like ITER.

However, it should be noted that, despite the success of the integrated modelling in predicting the core fusion peak performance, we could not predict the different behaviour of the density in T and D–T. The reason for this is that QuaLiKiZ, as most transport models presently available, cannot be applied in the edge transport barrier (ETB) of an H-mode plasma. Therefore, in the extrapolations from D to D–T plasmas we prescribed the transport in the ETB to obtain the same stationary density at the top of the pedestal [28], as indeed, because of the type-I ELM, it was the case for the baseline scenario in DTE1 and for the hybrid scenario in DTE2. This assumption was necessary because of the lack of a reduced transport model valid in the ETB for compound ELMs and for different plasma isotopic compositions and highlights the importance of reliable predictive modelling capabilities for transport in the ETB both between and during ELMs, which are still being developed. It should be also noted that, despite computationally expensive local gyrokinetic simulations (mostly linear) have recently started to shed light on the transport in the H-mode pedestal and its dependence on the isotope mass, reduced models that can be run to model a scenario in an integrated fashion and on time scales of the order at least of a few confinement times are still lacking.

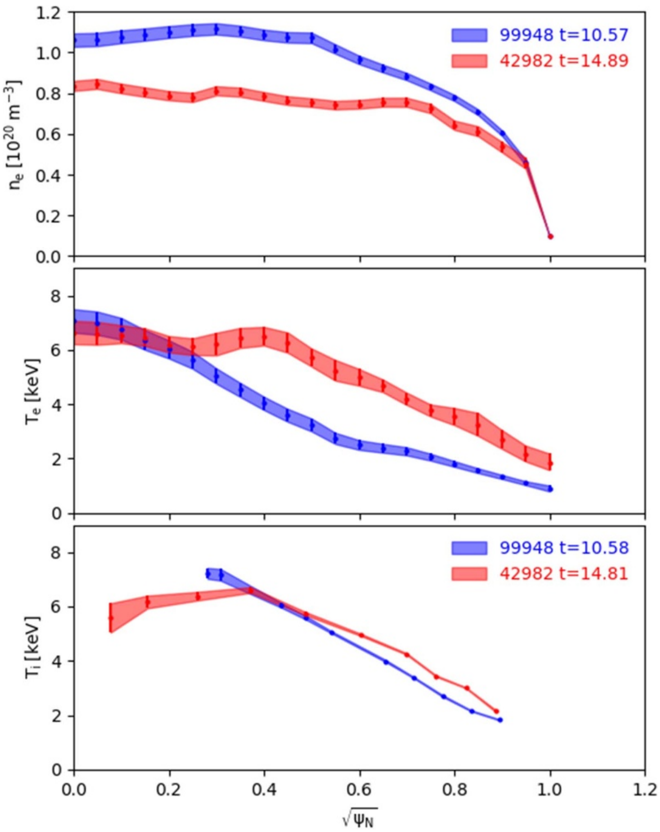

Figure 7. Comparison of electron density (top), electron temperature (middle) and ion temperature (bottom) profiles for JPN 99948 (3.5 MA/3.35 T, DTE2, D–T) and JPN 42982 (3.8 MA/3.8 T, DTE1, D–T).

Extrapolating the results obtained on JET developing a high-current high-fusion-performance scenario to ITER is not straightforward. Similarly to the baseline scenario on JET, ITER will operate at high Greenwald fraction (∼0.8), in a

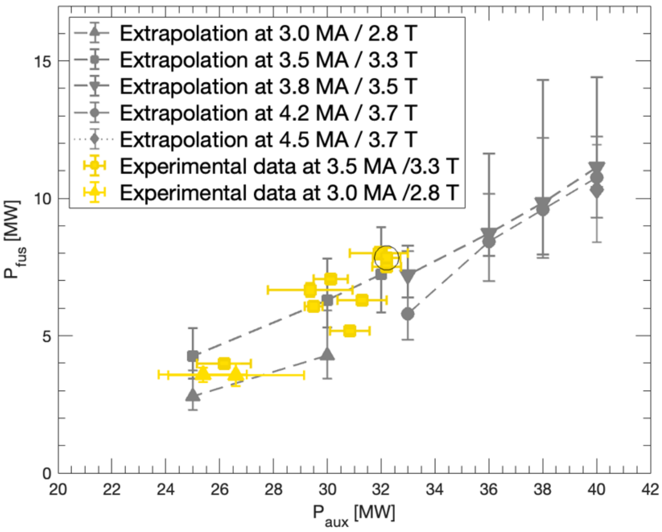

Figure 8. Predicted (gray) and measured (gold) peak fusion power as function of the additional heating power for the baseline scenario in D–T at 3.0 MA and 3.5 MA. Predictions were made with the QuaLiKiZ transport model before the start of DTE2. The black circle identifies JPN 99948, shown in figure 5. The horizontal error bars on the experimental points represent the RMS of the auxiliary heating power during the highest performance second around the fusion power peak, the vertical error bars on the predicted fusion power are obtained by increasing or decreasing the prescribed heat conductivity in the pedestal by 30%.

small ELM regime and, for the pre-burn phase, marginally above the L–H transition power threshold. On the other hand, unlike JET, ITER will operate with a semi-detached divertor and, because of the size of the machine and the intensity of the magnetic field, in conditions where the W prompt redeposition will likely be higher than on JET, making the migration of the W to the plasma core more difficult. Therefore, understanding the W transport mechanism from the sputtering at the plasma facing component to the separatrix is extremely important and modelling is ongoing to describe this phenomenon (see for example [30] and [31] and references within). The main reason for the impossibility to obtain sustained high performance at high current on JET was the incompatibility of a low enough density at the separatrix required not to degrade the confinement with the combined fuelling rate (gas plus pellet) required to sustain the ELM activity necessary to control the density and flush the W. Therefore, for ITER it will be paramount to develop a regime where high confinement, mitigated or suppressed ELMs, density control and W flushing/screening coexist. Moreover, it is not clear whether developing such a regime in D is directly transferrable to D–T, as demonstrated on JET. Finally, the experiments described in the paper underline the need for sufficient additional power to be installed in ITER in order to sustain for long enough the plasma density and temperature necessary to enter the D–T burning phase where 50% of the heating (mainly in the electron channel) will come from the fusion-born alpha particles.

6. Conclusions

In summary, a high-current baseline scenario for high fusion performance was successfully developed in D at JET at 3.5 MA/3.35 T by carefully optimizing the fuelling and ELM control scheme, involving a combination of pellet and gas puff, to achieve simultaneously good confinement and a compound ELM regime providing density control and impurity flushing. With an additional total heating power of ∼32 MW (NBI and ICRH) the scenario has the potential to deliver an average 7.0 MW of fusion power for 5 s when extrapolated to D–T.

However, when the scenario was translated to T and D–T, it could not be sustained for more than 1–2 s in T and 3 s in D–T. The physics reason for the loss of stationarity resides in the different behaviour of the ELMs and the density when the effective isotope mass is increased for the same fuelling rate. In particular, the improved particle confinement with higher effective isotope mass leads to higher pedestal and volume average density in T and D–T with respect to D. The higher density is associated with an increased radiated power, a diminished ELM activity and particle and impurity flushing and leads to a further increase in the density. The chain of events eventually terminates with a radiative collapse of the discharge and a H–L transition. It is worth noting that the loss of stationarity can start either with an uncontrolled density increase (due, for example, to different particle confinement depending on the plasma isotope mass) or with a cessation of the ELM activity (which can be due to insufficient particle throughput) or with a transient increase in radiated power (due, for example, to events inducing temporary enhanced W sputtering from the divertor) and the plasma is particularly vulnerable when it is not deeply in type-I ELM regime as it is the case in the baseline scenario at $I_p > 3.5$ MA.

The results presented in the paper show that in T and D–T, with the available power, it was possible on JET to achieve, but not to sustain a baseline scenario with good confinement for a plasma current $\geqslant$3.5 MA and with a W divertor, highlighting the difficulties underlying high-current operations in a machine with a metal wall. In particular, the control of the density at high plasma current, which, in H-mode, is largely the result of the ELM activity, is crucial to guarantee the stationarity of the scenario, even if the impurity concentration is initially kept at bay. Therefore, in view of extrapolating these results to future bigger machines, such as ITER, it is essential to understand, both from the theoretical and experimental point of view, particle and impurity transport for different isotopes, especially in the pedestal of an H-mode plasma, and the role of ELMs (not only type-I ELMs) in controlling the plasma density and the impurity concentration. Further analysis based on the results presented in this paper is in progress.

Data availability statement

The data that support the findings of this study are openly available at the following URL/DOI: https://doi.org/10.14468/n5jk-9h23 [32].

Acknowledgments

This work has been carried out within the framework of the EUROfusion Consortium, funded by the European Union via the Euratom Research and Training Programme (Grant Agreement No 101052200—EUROfusion) and from the EPSRC (Grant Number EP/W006839/1). This scientific paper has been published as part of the international project co-financed by the Polish Ministry of Science and Higher Education within the programme called 'PMW' for 2020–2023. This work was supported in part by grant PID2021-127727OB-I00, funded by the Spanish MCIN/AEI/10.13039/501100011033 and by ERDF "A way of making Europe". The Swiss contribution to this work has been funded by the Swiss State Secretariat for Education, Research and Innovation (SERI). Views and opinions expressed are however those of the authors only and do not necessarily reflect those of the European Union or the European Commission or SERI. Neither the European Union nor the European Commission nor SERI can be held responsible for them.

References

[1] Keilhacker M *et al* 1999 *Nucl. Fusion* **39** 209
[2] Jacquinot J *et al* 1999 *Nucl. Fusion* **39** 235
[3] Pasqualotto R, Nielsen P, Gowers C, Beurskens M, Kempenaars M, Carlstrom T and Johnson D 2004 *Rev. Sci. Instrum.* **75** 3891
[4] Gatu J M *et al* 2006 *Rev. Sci. Instrum.* **77** 10E702
[5] Kiptily V G *et al* 2024 *Nucl. Fusion* **64** 086059
[6] Hobirk J *et al* 2023 *Nucl. Fusion* **63** 112001
[7] Maslov M *et al* 2023 *Nucl. Fusion* **63** 112002
[8] Nunes I *et al* 2014 Compatibility of high-performance operation with JET ILW *Proc. 25th IAEA Fusion Energy Conf. (Russian Federation paper EX/9-2) (St. Petersburg, 13–18 October 2014)*
[9] Mailloux J *et al* 2022 *Nucl. Fusion* **62** 042026
[10] Loarte A for ITER Organisation, ITER Research Plan within the Staged Approach (Level III - Provisional Version) *Technical Report* ITR-18-003 (ITER Organization)
[11] Campbell D J and Collaborators I T E R 2012 Challenges in burning plasma physics: the ITER research plan *Proc. 24th Int. Conf. on Fusion Energy (San Diego, USA, 8–13 October 2012)* p ITR/P1-18
[12] Frassinetti L *et al* 2021 *Nucl. Fusion* **61** 126054
[13] Solano E R *et al* 2014 Effect of fuelling location on pedestal and ELMs in JET *Proc. 41st European Physical Society Conf. on Plasma Physics (Europhysics Conf. Abstracts) (Berlin, 23–27 June 2014)* vol 38F p 1.006
[14] Saibene G *et al* 2002 *Plasma Phys. Control. Fusion* **44** 1769
[15] Solano E R *et al* 2022 *Nucl. Fusion* **62** 076026
[16] Zotta V K *et al* 2022 Predictive modelling of D-T fuel mix control with gas puff and pellets for JET 3.5 MA baseline scenario *Proc. 48th European Physical Society Conf. on Plasma Physics (Europhysics Conf. Abstracts, Virtual Event) (27 June–1 July 2022)* vol 46A p 2a.115
[17] Van Eester D *et al* 2023 RF power as key contributor to high performance baseline scenario experiments in JET DD and DT plasmas in preparation for ITER *Proc. RF Power in Plasmas AIP Conf. Proc.* **vol 2984** p 030004
[18] Horton L D *et al* 1999 *Nucl. Fusion* **39** 993
[19] Hawryluk R J *et al* 1980 *An Empirical Approach to Tokamak Transport Physics of Plasmas Close to Thermonuclear Conditions* vol 1, ed B Coppi (CEC, Brussels) p 19
[20] Štancar Ž *et al* 2023 *Nucl. Fusion* **63** 126058
[21] Kim H-T, Sips A C C, Challis C D, Keeling D, King D, Joffrin E, Szepesi G, Buchanan J, Horton L D and Yuan X 2020 *Nucl. Fusion* **60** 066003
[22] Casson F J *et al* 2020 *Nucl. Fusion* **60** 066029
[23] Garcia J *et al* 2022 *Phys. Plasmas* **29** 032505
[24] Fajardo D, Angioni C, Casson F J, Field A R, Maget P and Manas P 2023 *Plasma Phys. Control. Fusion* **65** 035021
[25] Predebon I, Hatch D R, Frassinetti L, Horvath L, Saarelma S, Chapman-Oplopoiou B, Görler T and Maggi C F 2023 *Nucl. Fusion* **63** 036010
[26] Piron L, Challis C, Felton R, King D, Lennholm M, Lomas P, Piron C, Rimini F and Valcarcel D 2019 *Fus. Eng. Des.* **146** 133364
[27] Romanelli M *et al* 2014 *Plasma Fusion Res.* **9** 3403023
[28] Zotta V K *et al* 2022 *Nucl. Fusion* **62** 076024
[29] Bourdelle C, Citrin J, Baiocchi B, Casati A, Cottier P, Garbet X and Imbeaux F 2015 *Plasma Phys. Control. Fusion* **58** 014036
[30] Eriksson F *et al* 2024 *Nucl. Fusion* **64** 126033
[31] Kumpulainen H A, Groth M, Brezinsek S, Casson F, Corrigan G, Frassinetti L, Harting D and Romazanov J 2024 *Plasma Phys. Control. Fusion* **66** 055007
[32] Garzotti l 2025 Data from JET high current scenario development in D, DT and T *Dataset* (https://doi.org/10.14468/n5jk-9h23)